

## XMM-NEWTON OBSERVATIONS OF THE NUCLEI OF THE RADIO GALAXIES 3C 305, DA 240, AND 4C 73.08

DANIEL A. EVANS<sup>1,2</sup>, MARTIN J. HARDCASTLE<sup>3</sup>, JULIA C. LEE<sup>1,2</sup>, RALPH P. KRAFT<sup>2</sup>, DIANA M. WORRALL<sup>4</sup>, MARK BIRKINSHAW<sup>4</sup>,  
JUDITH H. CROSTON<sup>3</sup>

Draft version December 6, 2018

### ABSTRACT

We present new *XMM-Newton* EPIC observations of the nuclei of the nearby radio galaxies 3C 305, DA 240, and 4C 73.08, and investigate the origin of their nuclear X-ray emission. The nuclei of the three sources appear to have different relative contributions of accretion- and jet-related X-ray emission, as expected based on earlier work. The X-ray spectrum of the FRII narrow-line radio galaxy (NLRG) 4C 73.08 is modeled with the sum of a heavily absorbed power law that we interpret to be associated with a luminous accretion disk and circumnuclear obscuring structure, and an unabsorbed power law that originates in an unresolved jet. This behavior is consistent with other narrow-line radio galaxies. The X-ray emission of the low-excitation FRII radio galaxy DA 240 is best modeled as an unabsorbed power law that we associate with a parsec-scale jet, similar to other low-excitation sources that we have studied previously. However, the X-ray nucleus of the narrow-line radio galaxy 3C 305 shows no evidence for the heavily absorbed X-ray emission that has been found in other NLRGs. It is possible that the nuclear optical spectrum in 3C 305 is intrinsically weak-lined, with the strong emission arising from extended regions that indicate the presence of jet–environment interactions. Our observations of 3C 305 suggest that this source is more closely related to other weak-lined radio galaxies. This ambiguity could extend to other sources currently classified as NLRGs. We also present *XMM-Newton* and VLA observations of the hotspot of DA 240, arguing that this is another detection of X-ray synchrotron emission from a low-luminosity hotspot.

*Subject headings:* galaxies: active – galaxies: jets – galaxies: individual (3C 305, DA 240, 4C 73.08)

### 1. INTRODUCTION

Radio galaxies consist of twin jets of particles that are ejected from a compact region in the vicinity of a supermassive black hole, feeding into large-scale ‘plumes’ or ‘lobes’. There are two principal morphological classes of radio galaxies, low-power (Fanaroff-Riley type I, hereafter FRI) sources and high-power (FRII) sources Fanaroff & Riley (1974). FRI sources exhibit ‘edge-darkened’ large-scale radio structure, and modeling implies that initially supersonic jets in these sources decelerate to transonic speeds on  $\sim$ kpc scales before flaring into large plumes (e.g., Perucho & Martí 2007). FRII sources appear ‘edge-brightened’, and in these cases highly supersonic jets propagate out to large distances (often  $> 100$  kpc) from the core before terminating in bright hotspots and accompanying radio lobes. Observationally, the Fanaroff-Riley divide occurs at a 178-MHz radio power of  $\sim 10^{25}$  W Hz<sup>-1</sup> sr<sup>-1</sup>.

It is important to understand whether the kpc-scale Fanaroff-Riley dichotomy is determined by the interaction between the jet and its external hot-gas environment (e.g., Bicknell 1995), or rather is nuclear in origin and governed by differences in the properties of the accretion flow (Reynolds et al. 1996). The first observations of large samples of  $z < 0.1$  3CRR radio-galaxy nuclei with *Chandra* and *XMM-Newton* (Donato et al. 2004; Balmaverde et al. 2006; Evans et al. 2006) showed that FRI nuclei show no signs

of heavily absorbed X-ray emission that would be expected from standard AGN unification models (Urry & Padovani 1995), are dominated by emission from an unresolved jet (e.g., Worrall & Birkinshaw 1994; Balmaverde et al. 2006; Evans et al. 2006), and have highly radiatively inefficient accretion flows. Narrow optical-line FRII sources show evidence for heavily obscured ( $N_{\text{H}} > 10^{23}$  cm<sup>-2</sup>) nuclear X-ray emission that is associated with a radiatively efficient accretion flow, together with an unabsorbed component of jet-related emission (Evans et al. 2006; Hardcastle et al. 2006). FRII radio galaxies at higher redshift are consistent with such behavior (Belsole et al. 2006).

A significant breakthrough for understanding the physical origin of the FRI/FRII dichotomy came from *Chandra* and *XMM-Newton* observations of the population of *low-excitation radio galaxies* (LERGs), which have weak or no emission lines in their optical spectra (Hine & Longair 1979; Jackson & Rawlings 1997). Almost all FRI radio galaxies are LERGs, but there is a significant population of FRII LERGs at  $0.1 < z < 0.5$ . The X-ray spectra of LERGs, irrespective of their FRI or FRII morphology, are dominated by unabsorbed emission that can be associated with a parsec-scale jet, with no obvious contribution from accretion-related emission. These sources are likely to accrete in a radiatively inefficient manner (Hardcastle et al. 2006). On the other hand, high-excitation radio galaxies (HERGs – i.e., NLRGs, BLRGs, and quasars), which display prominent narrow or broad optical emission lines, have X-ray spectra that are consistent with standard unification models: they show evidence for luminous, radiatively efficient accretion disks, together with circumnuclear tori when the source is oriented close to edge-on with respect to the observer. HERGs tend to show evidence for additional hot dust over and above that of LERGs in their mid-IR spectra (e.g., Ogle et al. 2006; Birkinshaw et al., in

<sup>1</sup> Harvard University, Department of Astronomy, 60 Garden Street, Cambridge, MA 02138

<sup>2</sup> Harvard-Smithsonian Center for Astrophysics, 60 Garden Street, Cambridge, MA 02138

<sup>3</sup> School of Physics, Astronomy & Mathematics, University of Hertfordshire, College Lane, Hatfield AL10 9AB, UK

<sup>4</sup> University of Bristol, Department of Physics, Tyndall Avenue, Bristol BS8 1TL, UK

preparation), which is again consistent with reprocessing of luminous accretion-related emission by torus-like structure. Most high radio-power (FRII) sources are high-excitation radio galaxies. The distinct X-ray nuclear properties of low- and high-excitation radio galaxies, regardless of their large-scale FRI or FRII morphology, could be interpreted as implying that the Fanaroff-Riley dichotomy remains principally influenced by jet power and environment. The excitation dichotomy, on the other hand, is interpreted to be attributed to the radiative efficiency of the accretion flow (e.g., Hardcastle et al. 2006) and possibly related to the nature of the accreting material (Hardcastle et al. 2007a).

Here, we report new *XMM-Newton* observations of the nuclei of three  $z < 0.1$  3CRR radio galaxies — 3C 305, DA 240, and 4C 73.08. The three sources have 178-MHz radio powers that lie close to the FRI/FRII dividing luminosity (Table 1), plus a range of radio morphologies and optical emission-line characteristics. They are therefore good candidates for examining possible connections between the central engine and large-scale radio characteristics. This paper is organized as follows. In Section 2, we describe the optical and radio properties of the three sources. Section 3 contains a description of the data and a summary of our analysis. In Section 4, we report the results of our spectroscopic analysis of the sources. In Section 5, we describe VLA and *XMM-Newton* observations of the bright NE hotspot in DA 240. In Section 6, we interpret the observations in the context of our previous *Chandra* and *XMM-Newton* observations of 3CRR radio galaxies and discuss the optical emission-line characteristics of the sources. We end with our conclusions in Section 7. All results presented in this paper use a cosmology in which  $\Omega_{m,0} = 0.3$ ,  $\Omega_{\Lambda,0} = 0.7$ , and  $H_0 = 70 \text{ km s}^{-1} \text{ Mpc}^{-1}$ . Errors quoted in this paper are 90 per cent confidence for one parameter of interest (i.e.,  $\chi^2_{\text{min}} + 2.7$ ), unless otherwise stated.

## 2. OVERVIEW OF THE SOURCES

### 2.1. 3C 305

3C 305 is a  $z = 0.0416$  ( $d_L = 183 \text{ Mpc}$ ) narrow-line radio galaxy (Laing et al. 1983) with an unusually compact radio morphology that displays both FRI and FRII characteristics. MERLIN and VLA observations of the source (Heckman et al. 1982; Jackson et al. 2003; Morganti et al. 2005) show twin jets that each extend into radio lobes separated by  $\sim 4''$  (3.3 kpc). Laing et al. (1983) classify the source as an FRI-type radio galaxy. Optical emission-line studies of the circumnuclear environment of 3C 305 show an extended morphology (Heckman et al. 1982; Jackson et al. 1995), and a detailed comparison between the radio ejecta and [O II] gas observed with *HST* (Jackson et al. 1995) suggests that the gas has been shock-excited by the jet.

### 2.2. DA 240

DA 240 ( $z = 0.0356$ ,  $d_L = 157 \text{ Mpc}$ ) is a giant radio galaxy (GRG), the name given to the subclass of FRII sources with a projected radio extent in excess of 1 Mpc. Westerbork Synthesis Radio Telescope (WSRT) images of the source (Klein et al. 1994; Peng et al. 2004) show two hotspots, with the northeastern one 50 times brighter than the southwestern one. The northeastern hotspot has an unusual bifurcated structure, with what appears to be a radio jet entering a compact, primary hotspot, together with a fainter secondary hotspot feature. Optically, DA 240 is classified as a low-excitation radio galaxy (Laing et al. 1983).

### 2.3. 4C 73.08

4C 73.08 ( $z = 0.0581$ ,  $d_L = 258 \text{ Mpc}$ ) is another example of an FRII GRG. WSRT images (Mayer 1979; Klein et al. 1994) show a compact core accompanied by two hotspots. The brighter (western) hotspot is connected to the core by a bridge of radio emission. Both lobes show unusual protrusions toward the north and south. Optically, 4C 73.08 is classified as a narrow-line radio galaxy (Laing et al. 1983).

A summary of the properties of the three sources is given in Table 1.

## 3. OBSERVATIONS AND DATA REDUCTION

*XMM-Newton* observed 3C 305, DA 240, and 4C 73.08 as part of AO-5. We reprocessed the data with version 7.1.0 of the Scientific Analysis Software (SAS) using the standard pipeline tasks EMCHAIN and EPCHAIN. The data were filtered for PATTERN values  $\leq 12$  (MOS) and  $\leq 4$  (pn) and the bit-mask flags 0x766a0600 (MOS) and 0xfa000c (pn). These flagsets are equivalent to the standard flagsets #XM-MEA\_EM/EP but include out of field-of-view events and exclude bad columns and rows.

To check for intervals of high particle background, we extracted light curves from the CCD on which the source is located. The events were filtered to include only those with PATTERN=0 attributes and an energy range of 10–15 keV. The background was relatively low during the observations of 3C 305 and DA 240, meaning that no further filtering was required, especially given that we are performing spectral analyses of point sources. However, the observation of 4C 73.08 was heavily affected by flaring for almost the entire duration of the observation; indeed the MOS observation was truncated due to high background. We therefore chose filtering criteria of  $< 2.5 \text{ s}^{-1}$  (MOS) and  $< 25 \text{ s}^{-1}$  (pn) in the 10–15 keV band to remove the worst flaring but retain sufficient data to perform spectroscopy. Table 2 gives the details of the three *XMM-Newton* observations. All spectral fits include Galactic absorption.

The unresolved nuclei of all three sources are detected with *XMM-Newton*; in addition, there is a weak but clear detection of an X-ray source coincident with the bright NE hotspot of DA 240. We discuss the analysis of these X-ray features in the following two sections.

## 4. SPECTROSCOPIC ANALYSIS OF THE NUCLEI

### 4.1. 3C 305

We extracted the nuclear X-ray spectrum of 3C 305 from a source-centered circle of radius  $35''$ , with background sampled from a large off-source region on the same CCD as the target. There were sufficient counts in the spectra from each of the MOS1, MOS2, and pn cameras to perform a joint analysis for all three datasets. The spectra were grouped to a minimum of 20 counts per bin.

We initially attempted to fit the spectrum with a single, unabsorbed power law, but this achieved a poor fit ( $\chi^2 = 68.0$  for 33 dof). We found an acceptable fit ( $\chi^2 = 29.3$  for 31 dof) with the combination of an unabsorbed power law and thermal emission, characterized by an APEC model with  $kT = 0.69^{+0.10}_{-0.15} \text{ keV}$ , abundance fixed at 0.3 times solar, and normalization  $(3.78^{+1.06}_{-1.02}) \times 10^{-5} \text{ photons s}^{-1} \text{ cm}^{-2} \text{ keV}^{-1}$ . The best fitting parameters of the power law are  $\Gamma = 1.61^{+0.37}_{-0.38}$  and 1 keV normalization  $(1.45 \pm 0.44) \times 10^{-5} \text{ photons s}^{-1} \text{ cm}^{-2} \text{ keV}^{-1}$ . Adding additional components,

TABLE 1  
OVERVIEW OF THE THREE SOURCES

Source	Redshift	FR classification	Optical Excitation	Optical spectrum reference	178-MHz Luminosity Density ( $\text{W Hz}^{-1} \text{sr}^{-1}$ )	Galactic absorption ( $\text{cm}^{-2}$ )
3C 305	0.0416	I	NLRG	Liu & Kennicutt (1995)	$5.50 \times 10^{24}$	$1.69 \times 10^{20}$
DA 240	0.0356	II	LERG	Saunders et al. (1989)	$5.38 \times 10^{24}$	$4.36 \times 10^{20}$
4C 73.08	0.0581	II	NLRG	Saunders et al. (1989)	$9.94 \times 10^{24}$	$2.33 \times 10^{20}$

TABLE 2  
OBSERVATION LOG

Source	Obs ID	Observation date	Filter	Nominal exposure (ks)	Screened exposure (ks)
3C 305	0404050301	2006 August 08	Medium	11.4, 11.4, 9.8	11.4, 11.4, 9.8
DA 240	0404050101	2006 October 18	Medium	12.6, 12.6, 11.0	12.6, 12.6, 11.0
4C 73.08	0404050601	2007 April 28	Medium	4.5, 4.5, 13.9	3.4, 3.4, 4.7

NOTE. — Exposure times are quoted for the MOS1, MOS2, and pn cameras, respectively.

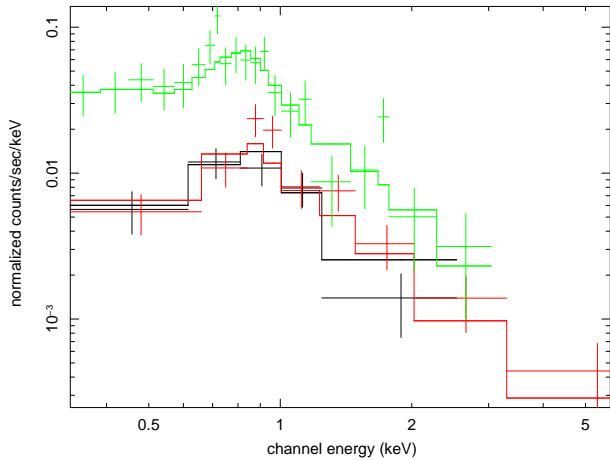


FIG. 1.— *XMM-Newton* MOS1 (black), MOS2 (red), and pn (green) spectrum of 3C 305. Also shown is the best-fitting model of an unabsorbed power law and thermal emission.

such as allowing the power law to be modified by additional absorption, failed to improve the fit (the best-fitting intrinsic absorption tended to zero). The thermal interpretation is supported by a *Chandra* observation of the source (PI: D. Harris), which shows resolved emission elongated  $3''$  either side of the nucleus along the direction of the jets. Indeed, the unresolved *Chandra* nuclear flux is 3 times lower than that which we measured with *XMM-Newton*. The *XMM-Newton* spectra and best-fitting model are shown in Figure 1.

#### 4.2. DA 240

We extracted the spectrum of the nucleus of DA 240 from a source-centered circle of radius  $35''$ , and extracted a background spectrum from a large off-source circular region on the same CCD. Only the spectrum from the pn camera had sufficient counts for an adequate spectral analysis. With the data grouped to 10 counts per bin, we found an acceptable fit ( $\chi^2 = 10.5$  for 9 dof) with a single unabsorbed power law of photon index  $1.91^{+0.54}_{-0.51}$  and 1 keV normalization  $(6.48^{+1.48}_{-1.51}) \times 10^{-6}$  photons  $\text{s}^{-1} \text{cm}^{-2} \text{keV}^{-1}$ . Allowing the power law to be modified by intrinsic absorption failed to improve the fit (the best-fitting  $N_{\text{H}}$  is zero). Additional components to our model also led to no statistically significant improvement in the fit. The spectrum, and best-fitting model, of a single, unabsorbed power law, are shown in Figure 2.

#### 4.3. 4C 73.08

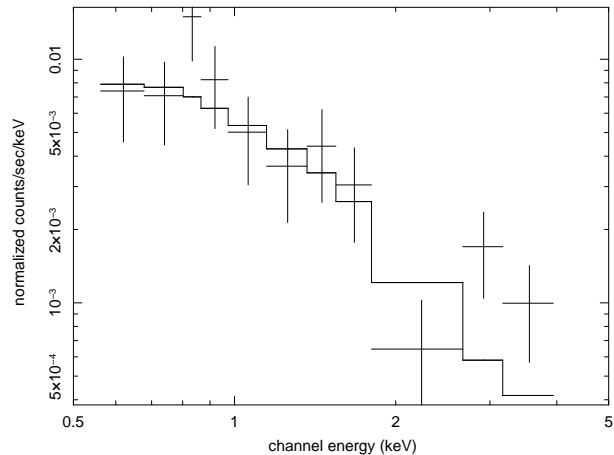


FIG. 2.— *XMM-Newton* pn spectrum of DA 240, together with the best-fitting model of an unabsorbed power law.

We sampled the nuclear spectrum of 4C 73.08 from a source-centered circle of radius  $35''$ , and extracted a background spectrum from a large off-source circular region on the same chip. We initially attempted to model the spectrum with a single, unabsorbed power law, but this achieved a poor fit ( $\chi^2 = 63.2$  for 15 dof), and we noticed significant residuals above  $\sim 4$  keV that clearly indicated the presence of an additional, heavily absorbed component. We achieved a good fit ( $\chi^2 = 7.2$  for 11 dof) to the spectrum with the sum of a heavily absorbed [ $N_{\text{H}} = (9.2^{+5.4}_{-2.9}) \times 10^{23} \text{cm}^{-2}$ ] power law of photon index frozen at 1.7, a Gaussian neutral, unresolved, Fe  $K\alpha$  line of equivalent width  $\sim 300$  eV (the Gaussian line is significant at the  $2\sigma$  level), and a second, unabsorbed, power law of photon index frozen at 2. There are insufficient counts to fit the power-law slopes, so we adopted values consistent with canonical values found in radio galaxies (e.g., Evans et al. 2004, 2006). The 1 keV normalizations of the power laws are  $(1.82^{+2.19}_{-1.00}) \times 10^{-3}$  photons  $\text{s}^{-1} \text{cm}^{-2} \text{keV}^{-1}$  and  $(1.90 \pm 0.47) \times 10^{-5}$  photons  $\text{s}^{-1} \text{cm}^{-2} \text{keV}^{-1}$ , respectively. Replacing the unabsorbed power law with a thermal component resulted in a worse fit to the spectrum ( $\chi^2 = 16.9$  for 10 dof). The spectrum and our best-fitting model are shown in Figure 3. The hotspots of 4C 73.08 are not detected in this short observation.

Table 3 summarizes the best-fitting spectral models to the X-ray spectra of 3C 305, DA 240, and 4C 73.08.

TABLE 3  
SUMMARY OF BEST-FITTING SPECTRA

Source (1)	Spectrum (2)	$N_{\text{H}}$ ( $\text{cm}^{-2}$ ) (3)	$\Gamma$ (4)	E (keV) (5)	$\sigma$ (keV) (6)	$kT$ (keV) (7)	$L_{(2-10\text{keV})}$ (Power Law) ( $\text{ergs s}^{-1}$ ) (8)	$\chi^2/\text{dof}$ (9)
3C 305	PL+TH	—	$1.61^{+0.37}_{-0.38}$	—	—	$0.61^{+0.10}_{-0.15}$	$(2.6 \pm 0.8) \times 10^{41}$	29.3/31
DA 240	PL	—	$1.91^{+0.54}_{-0.51}$	—	—	—	$(5.5 \pm 1.3) \times 10^{40}$	10.5/9
4C 73.08	$N_{\text{H}}(\text{PL}+\text{Gauss})+\text{PL}$	$(9.2^{+5.4}_{-2.9}) \times 10^{23}$	$\Gamma_1 = 1.7$ (f); $\Gamma_2 = 2$ (f)	$6.32 \pm 0.14$	0.01 (f)	—	$(5.7^{+6.9}_{-3.2}) \times 10^{43}$	7.2/11
		—	—	—	—	—	$(3.8 \pm 0.9) \times 10^{41}$	

NOTE. — Col. (1): Name of source. Col. (2): Description of best spectrum ( $N_{\text{H}}$ =Intrinsic absorption, PL=Power Law, Gauss=Redshifted Gaussian Line, TH=Thermal. Col. (3): Intrinsic neutral hydrogen column density. Galactic absorption has also been applied. Col. (4): Power-law photon index. Col. (5): Rest-frame Gaussian centroid energy. Col. (6): Gaussian linewidth. Col. (7): Temperature of thermal component. Col. (8): 2–10 keV unabsorbed luminosity of primary power law. Col. (9): Value of  $\chi^2$  and degrees of freedom. (f) Indicates parameter was frozen.

TABLE 4  
X-RAY AND RADIO LUMINOSITIES

Source (1)	Radio core luminosity density ( $\text{W Hz}^{-1} \text{sr}^{-1}$ ) and frequency (2)	1-keV soft luminosity density ( $\text{W Hz}^{-1} \text{sr}^{-1}$ ) (3)	178-MHz luminosity density ( $\text{W Hz}^{-1} \text{sr}^{-1}$ ) (4)	2–10 keV ‘accretion’ luminosity ( $\text{ergs s}^{-1}$ ) (5)	Core luminosity Reference (6)
3C 305	$< 3.21 \times 10^{20}$ (1.4 GHz)	$(3.1 \pm 0.9) \times 10^{15}$	$5.50 \times 10^{24}$	$< 1.0 \times 10^{42}$	Saripalli et al. (1997)
DA 240	$2.46 \times 10^{22}$ (5 GHz)	$(1.4 \pm 0.3) \times 10^{15}$	$5.38 \times 10^{24}$	$< 5.3 \times 10^{41}$	Tsien (1982)
4C73.08	$3.53 \times 10^{21}$ (5 GHz)	$(4.1 \pm 1.0) \times 10^{15}$	$9.94 \times 10^{24}$	$(5.7^{+6.9}_{-3.2}) \times 10^{43}$	Saripalli et al. (1997)

NOTE. — Col. (1): Name of source. Col. (2): Radio luminosity density of core. Col. (3): 1-keV unabsorbed luminosity density of soft X-ray component. Col. (4): 178-MHz VLA luminosity density. Col. (5): 2–10 keV unabsorbed X-ray ‘accretion-related’ luminosity. Obtained by direct fitting with free  $N_{\text{H}}$  (4C 73.08) and as a hidden component with  $N_{\text{H}}$  fixed at  $10^{23} \text{ cm}^{-2}$  (3C 305, DA 240). Col. (6): Reference for radio core luminosity density.

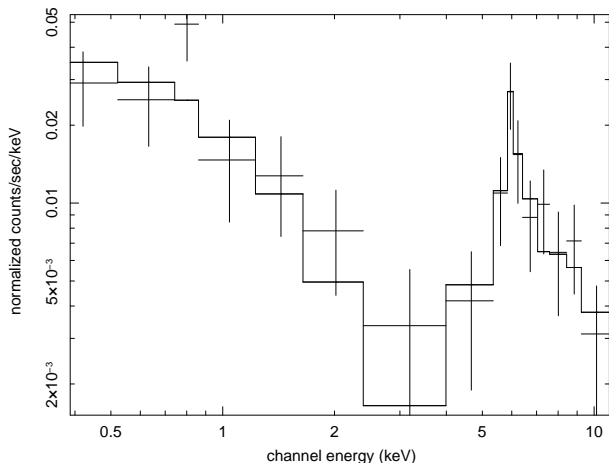


FIG. 3.— *XMM-Newton* pn spectrum of 4C 73.08. Also shown is the best-fitting model of a heavily absorbed power law, a neutral Fe  $K\alpha$  line, and a second, unabsorbed power law.

### 5. THE HOTSPOT OF DA 240

The bright NE hotspot of the giant radio galaxy DA 240 lies in the *XMM-Newton* field of view and is clearly detected in X-rays in our observation (Fig. 4). X-ray detections of the hotspots in relative low-luminosity radio sources like our targets are quite common in *Chandra* observations (e.g., Kraft et al. 2005; Hardcastle & Croston 2005; Kraft et al. 2007; Hardcastle et al. 2007b; Evans et al. 2008) and recently some bright hotspots have also been detected with *XMM-Newton* (Erlund et al. 2007; Goodger et al. 2008). It has been argued that that X-ray detections of low-luminosity hotspots such as those of DA 240 (whose NE hotspot has a 5-GHz radio luminosity of  $9 \times 10^{22} \text{ W Hz}^{-1} \text{sr}^{-1}$ ) are almost certainly due to synchrotron rather than inverse-Compton emission (see Fig. 5 of Hardcastle et al. 2004). If this is the case, X-ray detections of hotspots can give us important in-

formation about the relationship between the location of high-energy particle acceleration (traced by the X-ray) and the locations where low-energy particle and field energy densities are highest (traced by the radio synchrotron emission). The available evidence to date is that this relationship is complex; kpc-scale offsets are often found between the peaks of X-ray and radio emission (e.g., Hardcastle et al. 2007b).

The only radio image for DA 240 available to us at the start of our study was the WSRT 608-MHz image from the on-line atlas of low- $z$  3CRR sources<sup>5</sup>. This image has a resolution of  $34''$ , and so does not allow us to see details of the hotspot structure or its relationship to the X-ray emission. Accordingly we obtained a short observation of the hotspot with the VLA at 4.9 GHz under the exploratory time program. This observation (observation identifier AE163) was taken on 2007 May 18 when the VLA was in the process of moving between its D and A configurations. In addition, the EVLA antennas of the array were unavailable for most of the observation. As a result there were only 13 antennas available in the expected D-configuration arrangement, as opposed to the usual 27. Nevertheless we obtained an image with a resolution of  $7.5''$  and were able to detect and resolve the compact hotspot (Fig. 5). The radio emission coincident with the X-ray emission is resolved into two compact components aligned roughly N-S, with the brighter southern component having a radio flux density of 270 mJy and the fainter northern component at a level of  $\sim 90$  mJy, plus extended structure. Both the compact components are point-like at the resolution of our image; however, higher-resolution images (Tsien 1982) resolve the southern component, showing it contains at least two separate peaks. The peak of the X-ray emission is closest to the brighter component of the hotspot, but both components may be X-ray sources: the resolution of *XMM-Newton* is not good enough (particularly at this off-axis distance) to

<sup>5</sup> <http://www.jb.man.ac.uk/atlas/>

separate them. We used the default astrometry for both the VLA and *XMM-Newton* data to search for offsets between the radio and X-ray emission in the northern hotspot (the radio core is too far down the primary beam of the VLA for us to be able to use it to align the radio and X-ray frames). The X-ray emission appears to be offset by several kpc approximately in the direction of the nucleus. However the higher-resolution radio observation of Tsien (1982), which shows both the nucleus and hotspot, indicates that the brightest radio hotspot subcomponent (marked A by Tsien et al.) is separated by approximately  $8''$  ( $\sim 5.5$  kpc) from the brightest X-ray hotspot emission. This is consistent with our VLA observation in both sense and approximate offset with respect to the X-ray emission. Offsets this large, or larger, have been observed in other powerful radio galaxies (e.g., Erlund et al. 2007).

We extracted a spectrum for the hotspot from the pn data, using a  $30''$  radius circle as the source region and local background, and fitted it with a power-law model with Galactic absorption. It is well fitted ( $\chi^2 = 0.29$  for 2 d.o.f.) with a model with photon index of  $2.2 \pm 0.3$  and 1-keV unabsorbed flux density of  $7 \pm 1$  nJy. This flux density puts it among the brighter known X-ray hotspots (Hardcastle et al. 2004), very similar in flux density (though not luminosity) to the bright hotspot detected by Erlund et al. (2007) in the giant quasar 4C 74.26.

The steep X-ray spectrum and the possible offset between the radio and X-ray peak favor a synchrotron rather than inverse-Compton origin for the X-rays in this source. In the absence of optical measurements it is easy to fit a curved or broken synchrotron spectrum through the radio and X-ray data. Moreover, if we model the hotspot (normalizing using the observed radio flux for the brighter component) as a uniform sphere at equipartition with a radius of 1 kpc (which is consistent with the size reported by Tsien 1982 for the most compact component of the hotspot only) then the predicted inverse-Compton flux density, using the code of Hardcastle et al. (1998), is 3 orders of magnitude below that observed. All of the flux density from the hotspot would have to come from a region  $< 0.1$  pc in size, the magnetic field strength would have to be a factor  $\sim 30$  below the equipartition value, or some combination of the two would have to apply in order for the observed X-ray flux density to be produced by the synchrotron self-Compton model. Since DA240 is a low-excitation radio galaxy, the nuclear emission-line classification gives us no information about the orientation with respect to the line of sight, and so it is possible in principle that inverse-Compton emission could be boosted by a process which requires beaming and small angles of the jet to the line of sight (e.g., Georganopoulos & Kazanas 2003). However, an efficient role for beaming would imply a very large physical size ( $\gtrsim 4$  Mpc) for DA240, so we do not regard this model as probable, and we attribute the X-ray emission to synchrotron radiation. The relative brightness of the hotspot should make it a good target for follow-up radio and high-resolution X-ray observations aimed at understanding the details of high-energy particle acceleration in this source.

## 6. INTERPRETATION OF THE NUCLEAR SPECTRA

### 6.1. Overview of the spectra

The unabsorbed X-ray spectrum of the low-excitation FR II radio galaxy DA 240 is consistent with the other LERGs in the Hardcastle et al. (2006) sample, which observationally encompass both FRI and FR II radio galaxies. The high-

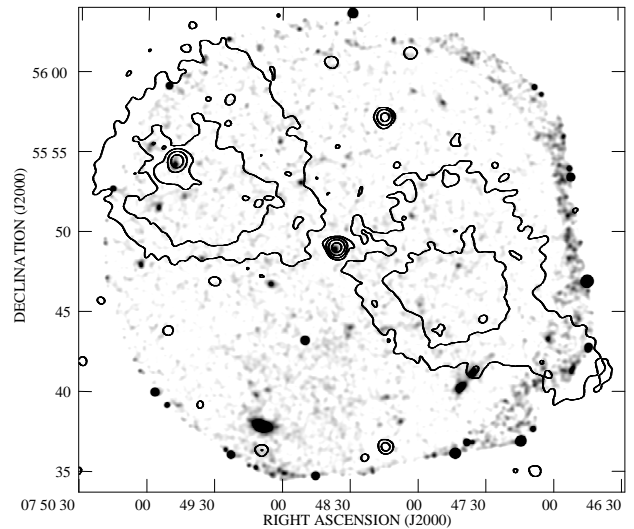


FIG. 4.— *XMM-Newton* observations of DA 240 in the MOS and pn cameras, co-added taking account of exposure and smoothed with a Gaussian of FWHM  $15.3''$ . Overlaid are contours from the  $34''$ -resolution 608-MHz WSRT map described in the text, at  $2 \times (1, 4, 16 \dots)$  mJy beam $^{-1}$ .

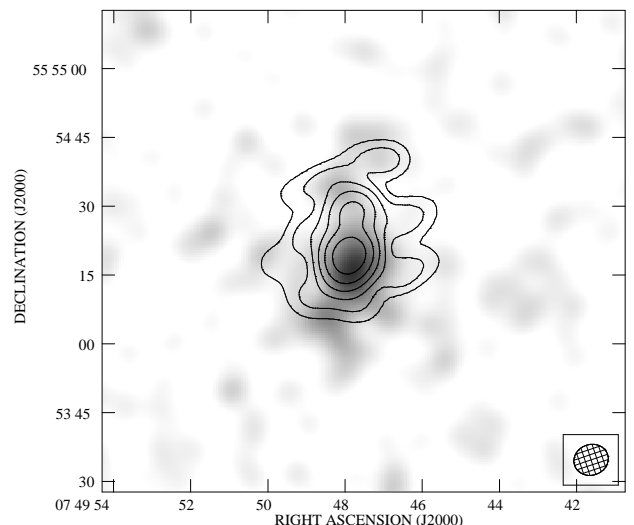


FIG. 5.— Co-added *XMM-Newton* observations of DA 240 as in Fig. 4, but smoothed with a Gaussian with FWHM  $6.1''$ . Overlaid are contours of our VLA data with  $7.5'' \times 6.7''$  resolution (major  $\times$  minor axis of restoring elliptical Gaussian) at  $4 \times (1, 2, 4 \dots)$  mJy beam $^{-1}$ . The 90% off-axis encircled energy radius of *XMM-Newton* at this location is  $\sim 1'$ .

excitation (narrow-line) FR II radio galaxy 4C 73.08 shows a heavily absorbed, luminous, component of X-ray emission, similar to the other narrow-line radio galaxies studied by Hardcastle et al. (2006). However, the spectrum of 3C 305 shows no evidence for the heavily absorbed X-ray emission that is characteristic of narrow-line radio galaxies. We return to this in Section 6.4.

### 6.2. The Radio Core–X-Ray Core Correlation

Figure 6 shows a plot of the 1-keV luminosity of the low-absorption power-law component against the core luminosity for our three sources (Table 4), together with the 3CRR sources presented in Evans et al. (2006) and Hardcastle et al. (2006). DA 240 and 4C 73.08 both lie close to the correlation between the radio and X-ray luminosities established

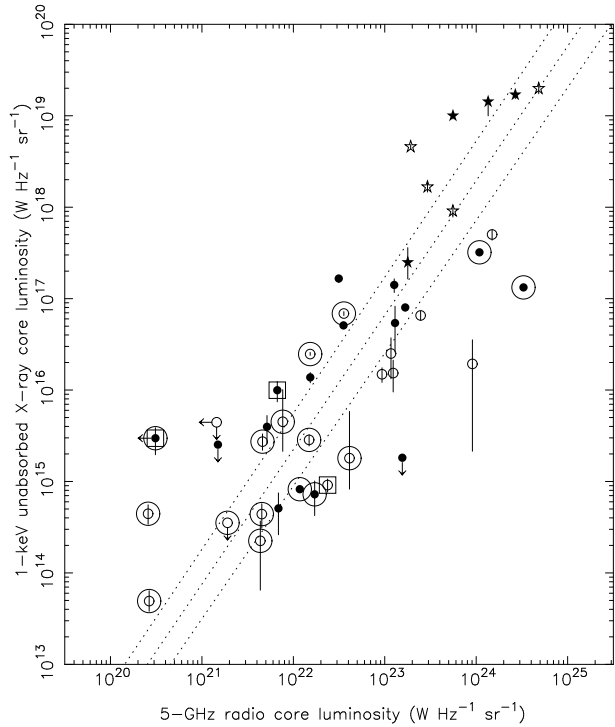


FIG. 6.— X-ray luminosity of the unabsorbed nuclear component for the three sources, together with combined  $z < 0.5$  sample (Evans et al. 2006; Hardcastle et al. 2006) as a function of 5-GHz radio core luminosity (Table 4). Open circles are LERG, filled circles NLRG, open stars BLRG, and filled stars quasars. Large surrounding circles indicate that a source is an FRI. The sources studied in this paper are indicated by surrounding boxes. Note that the core luminosity of 3C 305 is measured at 1.4 GHz. Where error bars are not visible they are smaller than symbols. Dotted lines show the regression line to all data and its  $1\sigma$  confidence range.

by, e.g., Fabbiano et al. (1984), Worrall & Birkinshaw (1994), and Hardcastle et al. (2006). On the other hand, 3C 305 lies somewhat away from the other data, though this is almost certainly due to the extended X-ray emission detected with *Chandra*. Indeed, the unresolved *Chandra* nuclear flux is 3 times lower than the *XMM-Newton* value, which would bring 3C 305 closer to established trendline in Figure 6. The radio–X-ray core correlation suggests a common origin of the two at the base of an unresolved jet, as has been extensively argued by, e.g., Worrall & Birkinshaw (1994), Hardcastle & Worrall (1999), Evans et al. (2006), Balmaverde et al. (2006) and Belsole et al. (2006).

### 6.3. Accretion-Related X-ray Emission

We now wish to consider any accretion-related X-ray emission. For 4C 73.08, as with the other narrow-line radio galaxies studied by Evans et al. (2006) and Hardcastle et al. (2006), we can take the accretion-related luminosity to be the unobscured luminosity of the heavily absorbed power-law component: this is supported by the presence of Fe  $K\alpha$  emission (e.g., Evans et al. 2006). The 2–10 keV accretion luminosity of 4C 73.08 ( $\sim 6 \times 10^{43}$  ergs  $s^{-1}$ ) is substantially larger than its jet-related luminosity ( $\sim 4 \times 10^{41}$  ergs  $s^{-1}$ ), as has been found with other NLRGs (e.g., Evans et al. 2006; Hardcastle et al. 2006).

In the cases of the LERG DA 240 and the (purported NLRG 3C 305), we followed the method of Evans et al. (2006) and assumed that, in addition to the dominant jet component of X-ray emission, there exists an additional ‘hidden’ component of accretion-related emission of photon index 1.7 that is

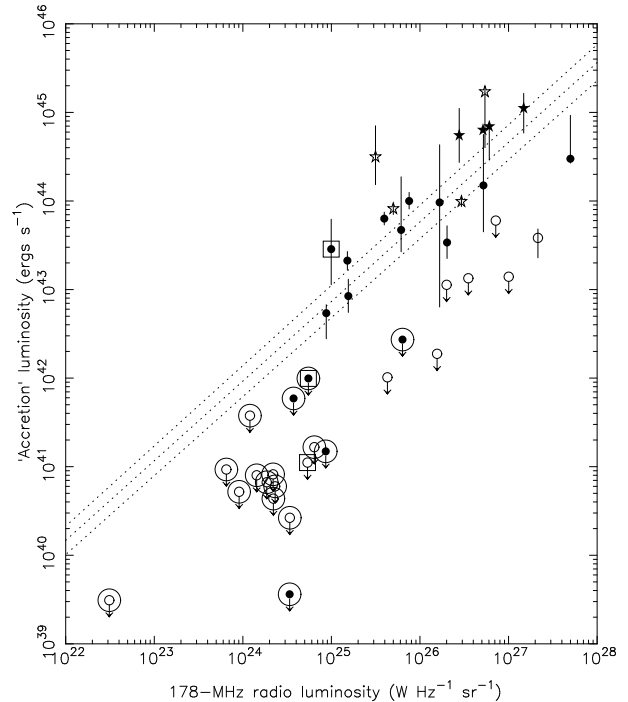


FIG. 7.— X-ray luminosity of the accretion-related component for the three sources, together with combined  $z < 0.5$  sample (Evans et al. 2006; Hardcastle et al. 2006) as a function of 178-MHz total radio luminosity (Table 4). Symbols are as in Fig. 6. Dotted lines show the regression line to the NLRGs only and its  $1\sigma$  confidence range.

obscured by a torus of intrinsic absorption  $10^{23}$   $cm^{-2}$ . We added this component to the best-fitting model, refitted the spectra, and determined the 90%-confidence upper limit to the 2–10 keV accretion-related luminosity to be  $5.3 \times 10^{41}$  ergs  $s^{-1}$  for DA 240 and  $1.0 \times 10^{42}$  ergs  $s^{-1}$  for 3C 305.

Figure 7 shows a plot of the 178-MHz and 2–10 keV accretion-related luminosities of the three sources (Table 4), together with those of the other  $z < 0.5$  3CRR sources studied by Evans et al. (2006) and Hardcastle et al. (2006). Figure 7 shows that the upper limit to the accretion-related components in the LERG DA 240, given our assumed absorbing column of  $10^{23}$   $cm^{-2}$ , lies below the trendline established for high-excitation (narrow-line) radio galaxies such as 4C 73.08. Of course, if no obscuring region is present in DA 240, as seems to be the case in other LERGs, then the luminosity of any accretion-related emission will be substantially lower than that shown. Alternatively, the accretion-related X-ray luminosity of LERGs can be made to lie in the region occupied by the HERGs, but this requires extremely high values of intrinsic absorption (Evans et al. 2004) that can be ruled out by infrared observations (e.g. Müller et al. 2004). The upper limit to the accretion-related luminosity of 3C 305 lies between the populations of low- and high-excitation sources in Figure 7, though as previously mentioned the *XMM-Newton*-measured unresolved core flux is overestimated by a factor  $\sim 3$  (see Section 4.1).

### 6.4. Optical Emission Line Classifications and Relationships to the Central Engine

In our previous studies of the X-ray properties of 3CRR radio sources we have used the Laing et al. (1983) optical emission-line classifications of low- and high-excitation radio galaxies. Laing et al. (1994) provided a quantitative definition of LERGs as having [OIII] equivalent widths of less than 3 Å

and [OIII]/H $\alpha$  line ratios  $> 0.2$ . A similar classification was given by Jackson & Rawlings (1997), with LERGs having [OIII] equivalent widths of less than 10 Å and/or [OII]/[OIII] line ratios  $> 1$ . However, these definitions of low- and high-excitation sources do not necessarily take into account the potentially *different* sources of ionizing radiation, their size scale, or their relationship to the AGN itself. This may lead to occasional ambiguities where sources are classified based on their emission-line characteristics. We discuss some of the issues here.

*HST* observations of the nuclei of radio galaxies have revealed the origin of the optical continuum emission and its likely relationship to any unresolved emission lines. In the case of LERGs, Chiaberge et al. (1999) and Hardcastle & Worrall (2000) showed that the correlations between the radio and optical continuum luminosities support the common origin of the two in the form of a jet. *HST* narrow-band imaging of LERGs (Capetti et al. 2005) showed that so-called Compact Emission Line Regions (CELRs) are commonplace, and that they are associated with the dominant source of ionizing photons, assumed to be the jet. Further, Chiaberge et al. (2002) argued that the dominant contribution to the optical emission in obscured high-excitation radio galaxies is the accretion disk. There is likely to be a substantial ionizing field in these sources that is directly related to the accretion process.

On larger scales, high-resolution *HST* emission-line images of the extended environments in radio galaxies (Privon et al. 2008) provide insights on the different components that constitute the kpc-scale narrow-line region (NLR) and  $\sim 10$  kpc-scale extended narrow-line region (ENLR). In addition to photoionization from the nucleus, jet–environment interactions may play a significant role in governing the energy budget of the NLR and ENLR, either in the form of collisional ionization or a radiative ‘autoionizing’ shock (e.g., Dopita & Sutherland 1995, 1996).

The different physical origins for optical line-emission in radio galaxies illustrate the difficulties in disentangling genuine AGN emission from that which is not directly related to the accretion process. An excellent case in point is the purported NLRG 3C 305, whose X-ray spectrum is consistent with that of a LERG, rather than a NLRG. *HST* [OII] observations of the extended emission-line environment in the source show that the majority of the [OII] emission lies just beyond the edge of the radio jet at a distance of 1.5'' from the core, and Jackson et al. (1995) suggested that it has been shock-excited by the jet. Several other FRI radio sources studied by Evans et al. (2006) and Hardcastle et al. (2006) also show optical spectra that may be attributed to their environments. Some of these lie at the centers of cooling-core clusters, in which significant amounts of optical line-emission might be expected that are not necessarily directly related to the central AGN. This may go some way to explaining the handful of other purported NLRGs in Figure 7 whose X-ray properties are more consistent with low-excitation sources.

The above arguments suggest that the emission-line classification of relatively weak-lined radio galaxies does not always reflect the nuclear accretion activity itself. We propose that only the combination of high-resolution optical spectroscopy, X-ray observations, and constraints from *Spitzer* mid-infrared observations of reprocessed emission in radio galaxies can reliably determine the structure of the central engine in radio-loud AGN. In the case of 3C 305, *Spitzer* observations would

enable us to distinguish between (1) a genuinely narrow-line radio galaxy that is obscured by a Compton-thick absorber (in which case the  $< 10$  keV X-ray continuum would show few, if any, signs of heavily absorbed emission), and (2) a low-excitation radio galaxy with a prominent extended emission-line environment. We will return to this point in subsequent publications (Birkinshaw et al., 2008, in prep.; Hardcastle et al. 2008, in prep.).

## 7. CONCLUSIONS

We have presented results from *XMM-Newton* observations of the nuclei of the radio galaxies 3C 305, DA 240, and 4C 73.08. We have shown the following:

1. The X-ray spectrum of the narrow-line FRII radio galaxy 4C 73.08 can be modeled as the sum of a heavily absorbed power law associated with a luminous accretion disk and circumnuclear obscuring structure, together with an unabsorbed component of X-ray emission that has a common origin with the radio emission at the base of an unresolved jet. This behavior is consistent with the other narrow-line FRII radio galaxies studied by Evans et al. (2006) and Hardcastle et al. (2006).
2. The nuclear X-ray spectrum of the FRII giant radio galaxy DA 240, optically classified as a low-excitation radio galaxy, can be modeled as a single, unabsorbed power law that is likely associated with emission from the parsec-scale jet. The upper limit to the X-ray luminosity of any additional, accretion-related emission suggests that the accretion process in DA 240 is substantially sub-Eddington and likely radiatively inefficient in nature.
3. The X-ray emission in the nucleus of the narrow-line radio galaxy 3C 305 can be modeled as an unabsorbed power law that originates at the base of the jet. However, it shows no evidence for heavily absorbed X-ray emission was found in the NLRGs studied by Evans et al. (2006).
4. We have discovered an X-ray counterpart to the NE hotspot of the giant radio galaxy DA 240. We argue that the emission process is overwhelmingly likely to be synchrotron emission. Because of the high X-ray flux of the hotspot, it is a good candidate for followup high-resolution X-ray observations.
5. We have discussed the different origins of optical emission lines in the nuclear and circumnuclear gaseous environments of radio galaxies. These include photoionization from the AGN accretion flow or parsec-scale jet, shock-excitation by the radio jet, or cooling gas in the centers of clusters. This may lead to occasional misclassification of genuinely weak-lined sources such as 3C 305 as high-excitation sources.
6. We therefore argue that there is not necessarily always a one-to-one correspondence between optical emission-line class (low- vs. high-excitation) and accretion-flow state (inefficient flow vs. standard thin disk), especially when low angular-resolution optical spectroscopy is used. We suggest that only the combination of high-resolution optical, X-ray, and infrared observations can reliably uncover the nature of the central engine in radio-loud AGN.

DAE gratefully acknowledges financial support for this work from NASA under grant number NNX06AG37G. MJH thanks the Royal Society for a Research Fellowship. We wish to thank the anonymous referee for valuable comments. We also thank Dan Harris and Francesco Massaro for useful discussions of the nuclear properties of 3C 305. This work is based on observations obtained with *XMM-Newton*, an ESA science mission with instruments and contributions directly funded by ESA Member States and NASA. The National Ra-

dio Astronomy Observatory is a facility of the National Science Foundation operated under cooperative agreement by Associated Universities, Inc. This research has made use of the NASA/IPAC Extragalactic Database (NED) which is operated by the Jet Propulsion Laboratory, California Institute of Technology, under contract with the National Aeronautics and Space Administration.

## REFERENCES

- Balmaverde, B., Capetti, A., & Grandi, P. 2006, *A&A*, 451, 35  
 Belsole, E., Worrall, D. M., & Hardcastle, M. J. 2006, *MNRAS*, 366, 339  
 Bicknell, G. V. 1995, *ApJS*, 101, 29  
 Burns, J. O., Schwendeman, E., & White, R. A. 1983, *ApJ*, 271, 575  
 Capetti, A., Verdoes Kleijn, G., & Chiaberge, M. 2005, *A&A*, 439, 935  
 Chiaberge, M., Capetti, A., & Celotti, A. 1999, *A&A*, 349, 77  
 Chiaberge, M., Capetti, A., & Celotti, A. 2002, *A&A*, 394, 791  
 Croston, J. H., Hardcastle, M. J., & Birkinshaw, M. 2005, *MNRAS*, 357, 279  
 Croston, J. H., Kraft, R. P., & Hardcastle, M. J. 2007, *ApJ*, 660, 191  
 Dopita, M. A., & Sutherland, R. S. 1995, *ApJ*, 455, 468  
 Dopita, M. A., & Sutherland, R. S. 1996, *ApJS*, 102, 161  
 Donato, D., Sambruna, R. M., & Gliozzi, M. 2004, *ApJ*, 617, 915  
 Erlund, M. C., Fabian, A. C., Blundell, K. M., Moss, C., & Ballantyne, D. R. 2007, *MNRAS*, 379, 498  
 Evans, D. A., Kraft, R. P., Worrall, D. M., Hardcastle, M. J., Jones, C., Forman, W. R., & Murray, S. S. 2004, *ApJ*, 612, 786  
 Evans, D. A., Hardcastle, M. J., Croston, J. H., Worrall, D. M., & Birkinshaw, M. 2005, *MNRAS*, 359, 363  
 Evans, D. A., Worrall, D. M., Hardcastle, M. J., Kraft, R. P., & Birkinshaw, M. 2006, *ApJ*, 642, 96  
 Evans, D. A., et al. 2008, *ApJ*, 657, 1057  
 Fabbiano, G., Trinchieri, G., Elvis, M., Miller, L., & Longair, M. 1984, *ApJ*, 277, 115  
 Fanaroff, B. L., & Riley, J. M. 1974, *MNRAS*, 167, 31P  
 Georganopoulos, M., & Kazanas, D. 2003, *ApJ*, 589, L5  
 Giovannini, G., Cotton, W. D., Feretti, L., Lara, L., & Venturi, T. 1998, *ApJ*, 493, 632  
 Goodger, J. L., Hardcastle, M. J., Croston, J. H., Kassim, N., & Perley, R. A. 2008, *MNRAS* in press  
 Gopal-Krishna, & Wiita, P. J. 2000, *A&A*, 363, 507  
 Hardcastle, M. J., & Croston, J. H. 2005, *MNRAS*, 363, 649  
 Hardcastle, M. J., & Worrall, D. M. 1999, *MNRAS*, 309, 969  
 Hardcastle, M. J., & Worrall, D. M. 2000, *MNRAS*, 314, 359  
 Hardcastle, M. J., Birkinshaw, M., & Worrall, D. M. 2001, *MNRAS*, 326, 1499  
 Hardcastle, M. J., Birkinshaw, M., & Worrall, D. M. 1998, *MNRAS*, 294, 615  
 Hardcastle, M. J., Harris, D. E., Worrall, D. M., & Birkinshaw, M. 2004, *ApJ*, 612, 729  
 Hardcastle, M. J., Evans, D. A., & Croston, J. H. 2006, *MNRAS*, 370, 1893  
 Hardcastle, M. J., Evans, D. A., & Croston, J. H. 2007a, *MNRAS*, 376, 1849  
 Hardcastle, M. J., Croston, J. H., & Kraft, R. P. 2007b, *ApJ*, 669, 893  
 Heckman, T. M., Miley, G. K., Balick, B., van Breugel, W. J. M., & Butcher, H. R. 1982, *ApJ*, 262, 529  
 Hine, R. G., & Longair, M. S. 1979, *MNRAS*, 188, 111  
 Jackson, N., Sparks, W. B., Miley, G. K., & Macchetto, F. 1995, *A&A*, 296, 339  
 Jackson, N., & Rawlings, S. 1997, *MNRAS*, 286, 241  
 Jackson, N., Beswick, R., Pedlar, A., Cole, G. H., Sparks, W. B., Leahy, J. P., Axon, D. J., & Holloway, A. J. 2003, *MNRAS*, 338, 643  
 Klein, U., Mack, K. H., Strom, R., Wielebinski, R., & Achatz, U. 1994, *A&A*, 283, 729  
 Kraft, R. P., Hardcastle, M. J., Worrall, D. M., & Murray, S. S. 2005, *ApJ*, 622, 149  
 Kraft, R. P., Birkinshaw, M., Hardcastle, M. J., Evans, D. A., Croston, J. H., Worrall, D. M., & Murray, S. S. 2007, *ApJ*, 659, 1008  
 Laing, R. A., Riley, J. M., & Longair, M. S. 1983, *MNRAS*, 204, 151  
 Laing, R. A., Jenkins, C. R., Wall, J. V., & Unger, S. W. 1994, *The Physics of Active Galaxies*, 54, 201  
 Ledlow, M. J., & Owen, F. N. 1996, *AJ*, 112, 9  
 Liu, C. T., & Kennicutt, R. C., Jr. 1995, *ApJS*, 100, 325  
 Mayer, C. J. 1979, *MNRAS*, 186, 99  
 Morganti, R., Oosterloo, T. A., Tadhunter, C. N., van Moorsel, G., & Emonts, B. 2005, *A&A*, 439, 521  
 Müller, S. A. H., Haas, M., Siebenmorgen, R., Klaas, U., Meisenheimer, K., Chini, R., & Albrecht, M. 2004, *A&A*, 426, L29  
 Ogle, P., Whysong, D., & Antonucci, R. 2006, *ApJ*, 647, 161  
 Peng, B., Strom, R. G., Wei, J., & Zhao, Y. H. 2004, *A&A*, 415, 487  
 Perucho, M., & Martí, J. M. 2007, *MNRAS*, 382, 526  
 Privo, G. C., O’Dea, C. P., Baum, S. A., Axon, D. J., Kharb, P., Buchanan, C. L., Sparks, W., & Chiaberge, M. 2008, *ApJS*, 175, 423  
 Protassov, R., van Dyk, D. A., Connors, A., Kashyap, V. L., & Siemiginowska, A. 2002, *ApJ*, 571, 545  
 Rawlings, S., & Saunders, R. 1991, *Nature*, 349, 138  
 Reynolds, C. S., di Matteo, T., Fabian, A. C., Hwang, U., & Canizares, C. R. 1996, *MNRAS*, 283, L111  
 Sambruna, R. M., Gambill, J. K., Maraschi, L., Tavecchio, F., Cerutti, R., Cheung, C. C., Urry, C. M., & Chartas, G. 2004, *ApJ*, 608, 698  
 Saripalli, L., Patnaik, A. R., Porcas, R. W., & Graham, D. A. 1997, *A&A*, 328, 78  
 Saunders, R., Baldwin, J. E., Rawlings, S., Warner, P. J., & Miller, L. 1989, *MNRAS*, 238, 777  
 Tsien, S. C. 1982, *MNRAS*, 200, 377  
 Urry, C. M., & Padovani, P. 1995, *PASP*, 107, 803  
 Whysong, D., & Antonucci, R. 2004, *ApJ*, 602, 116  
 Worrall, D. M., & Birkinshaw, M. 1994, *ApJ*, 427, 134  
 Worrall, D. M., Birkinshaw, M., & Hardcastle, M. J. 2001, *MNRAS*, 326, L7